Tanzania Journal of Engineering and Technology 2024, **43**(2):139 - 149
OPEN ACCESS articles distributed under Creative Commons Attribution Licence [CC BY-ND]
Websites: https://ajol.org/tjet; https://tjet.udsm.ac.tz

ISSN 1821-536X (**print**); ISSN 2619-8789 (**electronic**)
https://doi.org/10.52339/tjet.v43i2.997

Regular Research Manuscript

Perona-Malik Diffusion-Driven Regularization for Image Resolution Enhancement in Electrical Capacitance Tomography

Johnson Dismas, Nassor Ally†, Josiah Nombo, Alfred Mwambela, and Baraka Maiseli

Department of Electronics and Telecommunications Engineering, University of Dar es Salaam, P.O. Box 33335, Dar es Salaam, Tanzania.

†Corresponding author: naskindy@gmail.com; ORCID: 0000-0003-2085-8111

ABSTRACT

Electrical Capacitance Tomography (ECT) is a non-invasive promising method for monitoring industrial processes, such as oil-gas flow in pipelines and solid-gas flow in pneumatic systems. Despite its potential benefits, ECT generates poor-quality images, often used only for qualitative analysis. A non-linear relationship between measured capacitances and permittivity distribution and the ill-posedness of the sensitivity matrix elements causes this limitation. This hinders the applicability of ECT in monitoring online industrial process applications. This work proposes a reconstruction method based on a nonlinear diffusion function to generate high-quality images from the measured capacitance data from the ECT system. The diffusion regularization functional helps to remove noise and preserve semantic features. Experimental results reveal that the proposed method generates high-quality and visually appealing images with a 15% reduction in distribution error and a 10% increase in correlation coefficient compared to state-of-the-art methods such as linear back projection and projected landweber. This allows further investigation into how nonlinear anisotropic diffusion can improve the applicability of ECT systems in industrial control and monitoring.

ARTICLE INFO

Submitted: **Dec. 44, 2023**

Revised: **May 1, 2024**

Accepted: **June 15, 2024**

Published: **Aug. 2024**

Keywords: *Electrical capacitance tomography, Inverse problem, Nonlinear anisotropic diffusion, Image reconstruction, and Perona-Malik Model.*

INTRODUCTION

Electrical capacitance tomography (ECT) is a vital imaging technique to monitor the progress of industrial processes. This technique has a lower reconstruction time and is relatively inexpensive and can be used in harsh environments (Ghaly, Khan, et al., 2023). The usefulness of ECT as a viable image reconstruction tool depends on many factors, including spatial information of the generated images. Despite its advantages and wide applications, ECT systems generate poor images with lower spatial resolution, especially when used in pipeline and pneumatic systems (Tiwari et al., 2022). This limits the applicability of ECT reconstruction methods in practical industrial systems (Deabes & Amin, 2020). On the other hand, the ECT reconstruction problem is inherently ill-posed, hence prone to unstable and multiple solutions. Additionally, ECT electronics suffer from nonzero leakage currents, and associated methods produce a nonlinear mapping between capacitance and dielectric constant (Wang et al., 2020).

Numerous reconstruction methods have been proposed for the past few decades to

address the ECT problem (Sharifi et al., 2024) (Sun et al., 2023). Among the methods studied, Linear Back Projection (LBP) stands out as the most computationally efficient; however, it tends to produce images of lower quality (Nombo et al., 2021). Standard Tikhonov regularization effectively addresses the ill-posed nature of the problem but often results in images with reduced resolution (Suo et al., 2023). Landweber iteration achieves high-quality image reconstruction but suffers from slow convergence rates, rendering it impractical for real-time imaging applications (Rajan & Jose, 2022). Artificial neural networks and genetic algorithms optimize initial estimates to fit data optimally, yet they are prone to premature convergence, limiting their ability to achieve a globally optimal solution (Egwuche et al., 2023).

One of the promising approaches to improving the quality of the reconstructed images from the ECT system is to integrate the nonlinear anisotropic diffusion functional within the sensitivity matrix of the ECT model. This will assist in addressing the ill-posed problem. Nonlinear anisotropic diffusion functionals have demonstrated promising results in many image processing applications, such as denoising (Bua *et al*., 2024) and super-resolution image reconstruction (B. Maiseli & Abdalla, 2024). However, despite its nonlinear nature, the technique has not been applied in ECT image reconstructions. The proposed study leverages the non-linear attributes of both ECT and anisotropic diffusion models, by incorporating a non-linear diffusion functional within the sensitivity matrix of the ECT system. This will improve the quality of the images generated and enable the ECT system's applicability in online industrial process control and monitoring.

Among the studied diffusion methods, Perona and Malik diffusion functional has remained popular since its inception (Perona & Malik, 1990). This function performs uniform regularization across image regions, ensuring effective recovery and protection of semantic features like edges and contours. Compared with other regularizers, such as Charbonnier (Charbonnier et al., 1994) and Total Variation (Rudin et al., 1992). Perona-Malik has desirable mathematical properties, including robustness in noise and outlier rejection. Considering its promising performance in other image processing fields (Bua et al., 2024; Gobbino & Picenni, 2024; B. J. Maiseli, 2020; Rafsanjani et al., 2016), this study proposes an image reconstruction method based on Perona-Malik nonlinear diffusion functional. Results from a series of experiments demonstrate that the proposed method offers an improved performance, by generating images with appreciable salient features. Experimental results reveal that the proposed method generates high-quality and visually appealing images with a lower distribution error and high correlation coefficient compared to state-of-the-art methods.

METHODS AND MATERIALS

Description of the ECT Measurement Process

The ECT measurement process involves several steps from sensing to image reconstruction to facilitate the non-invasive imaging of the interior of the process under observation. The measurement process is divided into three main stages: sensing, signal processing, and image reconstruction (Figure 1).

The sensing unit consists of strategically placing an array of electrodes around the periphery of the object to be imaged, typically arranged around the inner wall of a pipe or container. This configuration ensures complete coverage of the sensing region. Capacitance measurements are taken by sequentially exciting pairs of electrodes with an AC signal while measuring the resulting capacitance between them. Each pair of electrodes acts as a transmitter and receiver, and this

process is repeated for all possible electrode pairs to gather a complete set of capacitance data (Li et al., 2023).

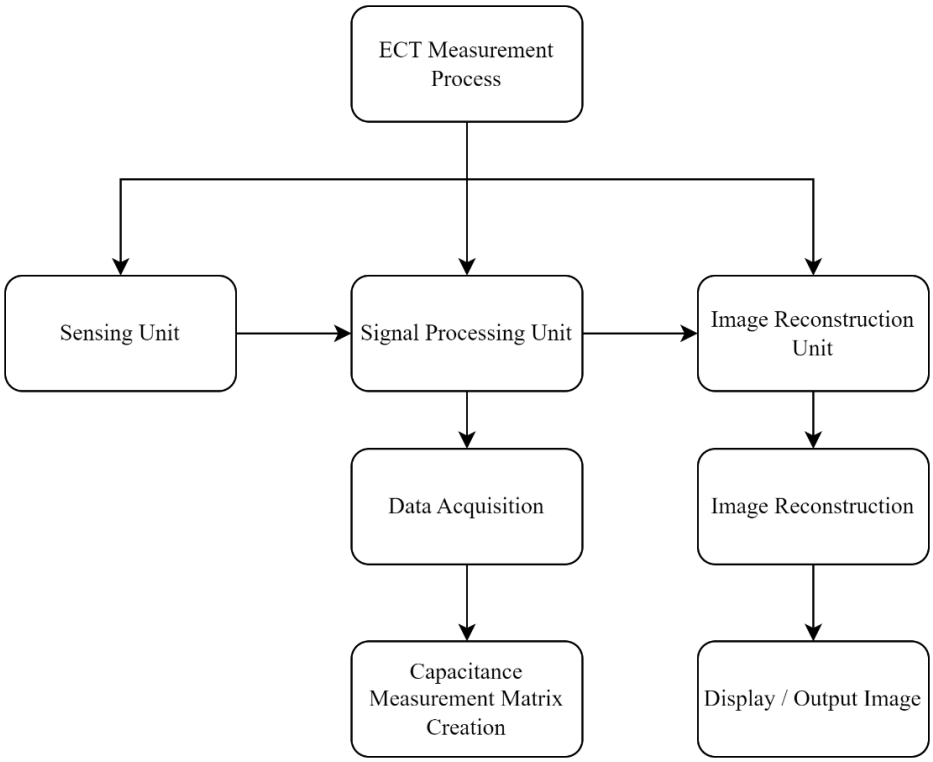

Figure 1: Description of the ECT measurement process.

The signal processing deals with the collection and analysis of measured capacitances. A switching matrix is used to sequentially select electrode pairs, ensuring comprehensive data acquisition (Mousazadeh et al., 2024). The weak capacitance signals are then amplified and filtered to enhance signal quality and reduce noise interference. These analogue signals are converted into a digital format using high-resolution analogue-to-digital converters, enabling subsequent digital processing and analysis (Hussain et al., 2023). The collected digital data forms a measurement matrix representing the capacitance values for all electrode pairs, serving as the input for the image reconstruction algorithms (Ghaly, Shalaby, et al., 2023).

A reconstruction unit is a computer in which image reconstruction algorithms are implemented. Its main function is to convert the measured capacitance data into an image. The conversion process involves calculating permittivity values for each pixel using measured capacitance data. The process is achieved through mathematical methods for solving inverse problems. Results are represented as visual images, and the process is called image reconstruction. There is no general method for solving the ECT inverse problem, different techniques have been developed by researchers which can be classified mainly into direct (single-step) techniques in which the image is obtained from measured capacitance in one mathematical step; and iterative techniques which a set of objective functions are optimized iteratively. In most image reconstruction techniques; whether single-step or iterative; the sensitivity matrix is used for forward or backward projection between the capacitance measurements and the reconstructed image. The sensitivity matrix is a linearization of the non-linear field to

physical property distribution (Dimas et al., 2024).

Diffusion-Based Regularization for Improved ECT Image Reconstruction

The ECT image reconstruction process involves solving two computational problems: forward and inverse (Huang et al., 2022). The forward problem is a simplified model of the ECT system and computes the capacitance values from a given permittivity distribution. The problem is defined as

$$C = SG \quad (1)$$

where G is an $N \times 1$ a dimensional vector representing an image vector, N is the number of pixels in the image, C is an $M \times 1$ a dimensional vector indicating the normalized capacitance values, M is the number of capacitance measurements, and S is an $M \times N$ field sensitivity matrix, which reflects the effect of permittivity distribution at each pixel on the inter-electrode capacitance. Without loss of generality, equation (1) can be written as

$$S^T C = S^T S G \quad (2)$$

and re-organized as

$$G = (S^T S)^{-1} S^T C \quad (3)$$

The ECT inverse problem aims to estimate G from the given capacitance data. However, in most cases, S is a non-square matrix that does not have a direct inverse, making the system ill-posed (Deabes & Amin, 2020). To address the problem, various reconstruction methods and regularization techniques have been proposed.

The term $S^T S$ in (3) is a non-invertible matrix, leading to degenerative solutions. Therefore, a regularization component can be introduced into the equation to address the problem. Subsequently, applying a regularization term, (3) becomes:

$$G = (S^T S + \mu I)^{-1} S^T C \quad (4)$$

where $\mu > 0$ is a regularization parameter and I denote the identity matrix of dimension the same as the matrix $S^T S$.

The proposed method formulation originates from the ECT reconstruction model (4) and the Perona-Malik energy functional (5).

$$\rho(S) = \frac{K^2}{2} \log(1 + S^2) \quad (5)$$

where s denotes an image gradient and K represents the gradient-thresholding parameter that should be manually tuned for better reconstruction results. The convexity property of (5) gives $\rho(S)$ the ability to generate desirable optimal solutions. The second derivative test, $\rho''(s) \geq 0$, is often a preferred technique to test for the convexity of an equation. Therefore,

$$\rho''(S) = \frac{K^2(1-S^2)}{(1+S^2)^2} \quad (6)$$

Equation (6) becomes convex when $1 - S^2 \geq 0$ or $S \leq 1$. We adhered to this important condition in the implementation of our method to ensure the stability and convexity of the evolving ECT solution.

Applying the Euler-Lagrange equation to (6), subjecting the resulting equation to a dynamical system, and incorporating a fidelity term give the anisotropic diffusion equation (Maiseli, 2020)

$$\frac{\partial S}{\partial t} = \nabla \left(\frac{1}{1+\left(\frac{|\nabla S|}{K}\right)^2} \nabla S \right) - \mu \, (S - S_o) \quad (7)$$

where λ, fidelity parameter, maintains a balance between reconstructing ECT image, S, and the original raw data (initial measurements, S_o). This equation suits many image processing applications, such as denoising, super-resolution, and inpainting. In our case, the equation was used to regularize the ECT solution. Specifically, the regularization component of (7) was encapsulated into (4), the re-organized version of (8), to form the Perona-Malik diffusion-driven regularization for image resolution enhancement in ECT (PMECT)

$$G = \left(S^T S + \mu \nabla \left(\frac{1}{1+\left(\frac{\nabla S}{K}\right)^2} \nabla S \right) \right)^{-1} S^T C \quad (8)$$

The value of the regularization parameter, μ, in (7) greatly affects the quality of the final reconstructed images. A moderate value of μ yields a good estimate of the

permittivity distribution. The solution is, in addition, significantly impacted by the capacitance measurement's inaccuracy. The capacitance error increases but the approximation error decreases with a high value of the regularization parameter. Discretizing (8) for computer implementation gives the iterative equation (9):

$$G_{ij}^{n+1} = G_{ij}^{n} + \Delta t \left(\left(S_{ij}^{T}\right)^{n} S_{ij}^{n} + \mu \nabla \left(\frac{1}{1+\left(\frac{\nabla S_{ij}^{n}}{K}\right)^{2}} \nabla S_{ij}^{n} \right) \right)^{-1} \left(S_{ij}^{T}\right)^{n} C_{ij}^{n} \quad (9)$$

where (i, j) is the spatial pixel position in the grid fabric of a reconstructing image, and n denotes the iteration number; the parameters were set as follows: $\Delta t = 0.25$, and μ=0.05. Equation (9) was implemented in MATLAB software.

Experimental Setup and Evaluation Criteria

Several experiments were conducted to evaluate the efficiency of the Perona-Malik-ECT (PMECT) algorithm. The ECT system was configured as an eight-electrode circular sensor with a pipeline divided into 900 units. three flow types, namely annular, stratified, and bubble were used. Image reconstruction algorithms were implemented using MATLAB. Qualitative and quantitative metrics were used to evaluate the efficacy of various methods. In the former evaluation metric, the visual results of the reconstructed images generated by different algorithms were subjectively compared. To quantify the quality of the results, we used an image distribution error (DE), defined as

$$\mathrm{DE} = \frac{1}{N}\sum_{i=1}^{N} \left| G_i^{rec} - G_i^{ref} \right| \quad (10)$$

where G_i^{rec} and G_i^{ref} are, respectively, the reference and reconstructed image vectors for an image element i, and N represents the total number of pixels of the reconstructed image. Lower DE signals better results in reservoir management in oil industries, for example, the desired DE should be less or equal to 10% (Almutairi et al., 2020). In addition, we used the correlation coefficient (CC) between reference and reconstructed images. This quality metric is defined as

$$\mathrm{CC} = \frac{\sum_{e=1}^{M} \left(\hat{G}(e) - \underline{\hat{G}}(e)\right)\left(G(e) - \hat{G}(e)\right)}{\sqrt{\sum_{e=1}^{M} \left(\hat{G}(e) - \underline{\hat{G}}(e)\right)^{2} \sum_{e=1}^{M} \left(\hat{G}(e) - \underline{\hat{G}}(e)\right)^{2}}} \quad (11)$$

where $\underline{G}$ and $\underline{\hat{G}}$ represent the average values of G and $\hat{G}$. The value of CC ranges between 0% and 100% and represents the degree of deviation of the reconstructed image from the true distribution. The quality of the reconstructed image increases with CC.

RESULTS AND DISCUSSION

Figure 2 provides a qualitative analysis of images reconstructed using Linear Back Projection (LPB), Projected Landweber (PLAND), and the proposed method (PMECT). The reconstructed images using PMECT closely resemble the true reference images. Specifically, the PMECT method generates images with higher resolution with a clear definition of boundaries. This superior performance of PMECT highlights its potential as a more effective ECT reconstruction technique, promising improved industrial process monitoring applications.

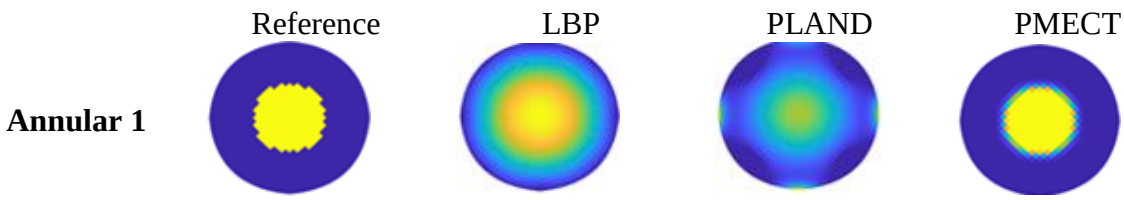

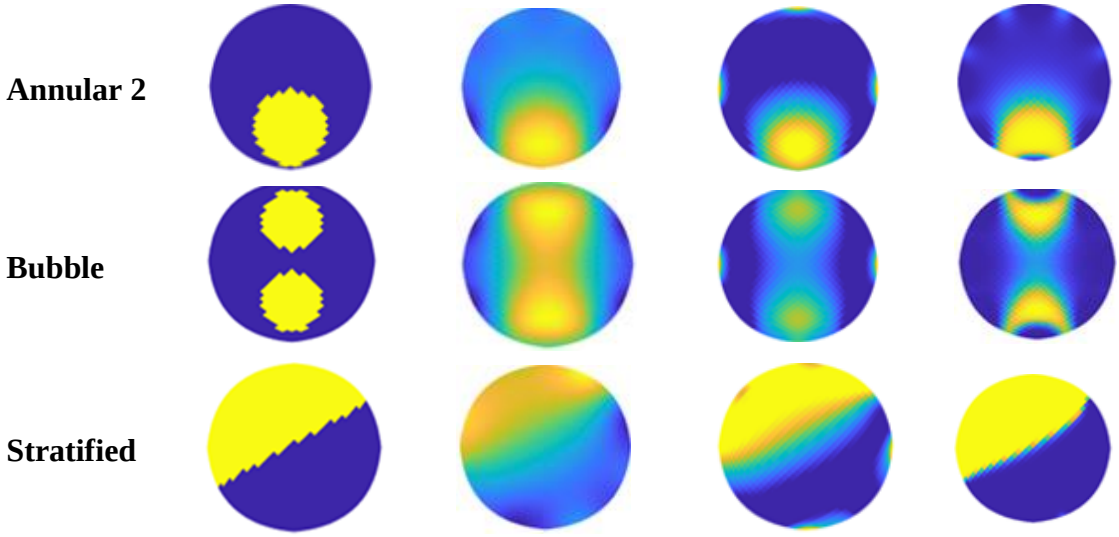

Figure 2. Qualitative Comparison of Reconstructed Images from Linear Back Projection (LPB), Projected Landweber (PLAND) and PMECT.

To further assess the performance of the proposed method, the evaluation was expanded to cover the full component fraction range for annular and stratified flows. Figure 3 presents the distribution error (DE) as a function of the Reference Gas Fraction (%) for LPB, PLAND, and PMECT for annular flow. The DE for the LBP shows a significant error margin across most reference gas fractions. Starting at approximately 0.1 DE at 0% gas fraction, the error peaks between 0.2 and 0.25 from 20% to 90% gas fractions, indicating substantial deviations from the reference values before tapering back to 0.1 at 100% gas fraction. Similarly, the PLAND method exhibits a high DE trajectory equivalent to the LBP, though slightly lower. The DE begins at 0.1 at 0% gas fraction, peaks just below 0.25 between 20% and 90%, and returns to 0.1 at 100%. In contrast, the PMECT method shows superior performance, maintaining a consistently low DE throughout the reference gas fraction range. Beginning below 0.05 at 0%, the DE remains under 0.1 for the majority of the spectrum, only slightly exceeding this threshold around the 80% gas fraction mark. The REF line at 0.1 DE serves as a benchmark, highlighting the acceptable error margin. Notably, both LBP and PLAND methods frequently surpass this benchmark, reflecting their lower accuracy and reliability. On the other hand, the PMECT method remains predominantly below this reference line, underscoring its robustness and precision.

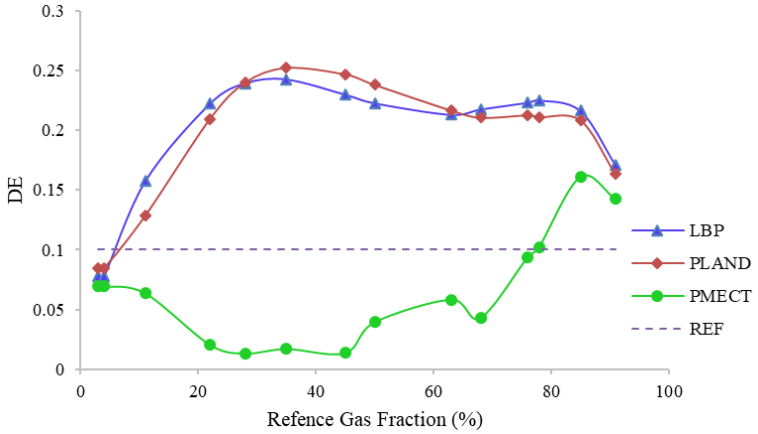

Figure 3. DE for the full component fraction range for annular flow.

Figure 4 presents the distribution rrror (DE) as a function of the Reference Gas Fraction (%) for stratified flow for LBP, PLAND, and PMECT, alongside a reference line (REF) set at a DE of 0.1. The LBP method exhibits a significant DE across most reference gas fractions, beginning around 0.1 at 0% gas fraction, peaking above 0.2 between 20% and 80%, and then tapering off towards the end. The PLAND method follows a similar trend, though with slightly lower DE values than LBP. The DE starts at 0.1 at 0% gas fraction, peaks just below 0.2 around the mid-range, and decreases back to around 0.1 towards 100% gas fraction. In contrast, the PMECT method shows a noticeably lower DE across the entire range. The DE starts below 0.05 at 0% gas fraction, remains significantly lower than both LBP and PLAND throughout, and only briefly approaches the REF line at certain points. The REF line at 0.1 DE serves as a benchmark for acceptable error levels. Both LBP and PLAND methods frequently surpass this threshold, indicating higher error rates and less reliable reconstructions. Conversely, the PMECT method stays predominantly below this benchmark, underscoring its enhanced accuracy and reliability. Figure 5 shows the correlation coefficient (CC) as a function of the Reference Gas Fraction (%) for annular flow. The LBP method quickly rises to approximately 0.8 by 20% gas fraction and maintains this value with slight fluctuations. The PLAND method starts with a negative CC at 0% but aligns with the LBP method from 20% gas fraction onward, stabilizing around 0.8. In contrast, the PMECT method starts close to 1.0 at 0% gas fraction and maintains a consistently high CC of around 0.9 throughout the range. This indicates superior performance and reliability. The REF line at 1.0 represents the ideal correlation. While the LBP and PLAND methods frequently fall below 0.9, the PMECT method stays significantly closer to this benchmark, highlighting its superior accuracy.

Figure 6 presents the correlation coefficient (CC) as a function of the stratified flow's reference gas fraction (%). The PMECT method consistently shows the highest CC values, indicating superior performance in accurately reconstructing the reference gas fraction. The LBP method generally performs better than PLAND, but both exhibit lower CC values compared to PMECT. At low reference gas fractions (0% to 20%), PMECT quickly surpasses a CC of 0.8. LBP shows a gradual increase, reaching about 0.8, while PLAND starts lower around 0.6 and increases more slowly. In the mid-range (20% to 80%), PMECT maintains high CC values, peaking around 0.9. LBP remains stable around 0.8, and PLAND hovers around 0.7 to 0.75 with more variability. At high reference gas fractions (80% to 100%), PMECT continues to outperform, with CC values close to 1. LBP and PLAND show a decline in performance but maintain CC values above 0.7. None of the methods achieve a perfect CC of 1, but PMECT comes closest, especially at higher gas fractions.

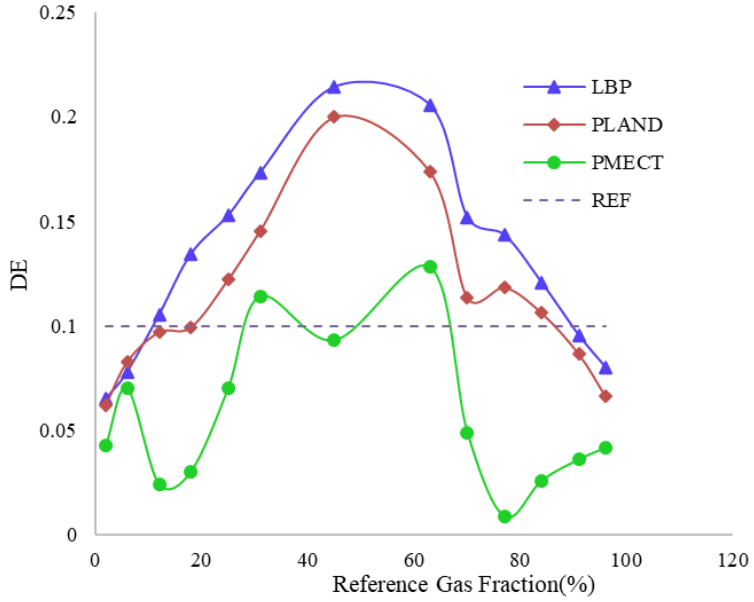

Figure 4. DE for the full component fraction range for stratified flow.

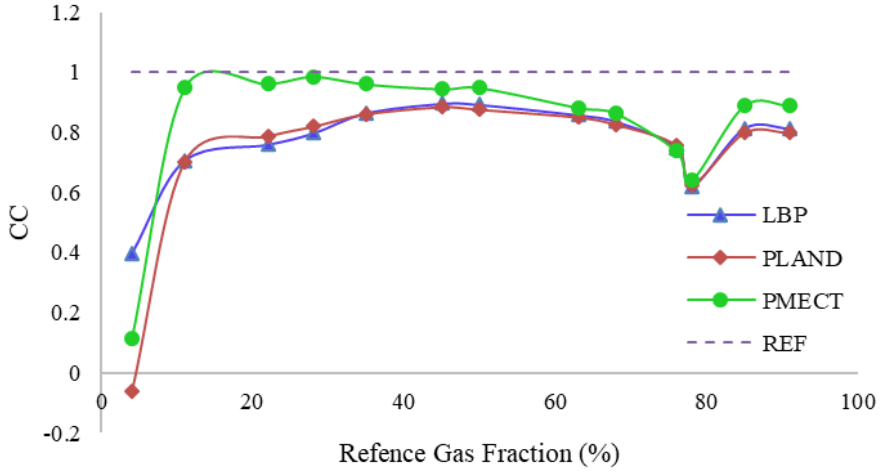

Figure 5. CC for the full component fraction range for annular flow.

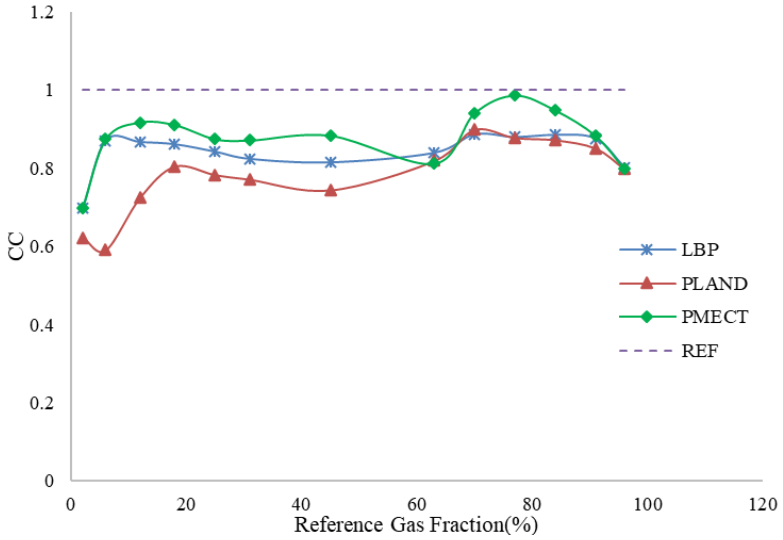

Figure 6: CC for the full component fraction range for stratified flow.

In summary, the PMECT method performs better in image reconstruction than the Linear Back Projection (LBP) and Projected Landweber (PLAND) methods. PMECT produces images with higher resolution and clearer boundary definition, closely resembling true reference images. It maintains a consistently low distribution error (DE) across various gas fractions for both annular and stratified flows, with an average DE difference of 15% lower than LBP and PLAND. Additionally, PMECT achieves the highest correlation coefficient (CC) values, with an average CC improvement of 10% over LBP and PLAND, indicating its robustness and precision. Overall, PMECT emerges as a more accurate and reliable ECT reconstruction technique, offering significant advantages for industrial process monitoring applications.

CONCLUSION

The Perona-Malik diffusion-driven regularization method significantly improves image resolution in Electrical Capacitance Tomography (ECT) applications. Experimental evaluations demonstrated a marked 15% reduction in distribution error (DE) and a 10% increase in the correlation coefficient (CC) for PMECT as compared to conventional reconstruction methods such as Linear Back Projection (LBP) and Projected Landweber (PLAND). By integrating nonlinear anisotropic diffusion within the sensitivity matrix of the ECT model, the proposed method effectively addresses the ill-posed nature of the inverse problem, thereby enhancing the fidelity and robustness of the reconstructed images. This improved performance is essential for monitoring industrial applications, where accurate and reliable image reconstruction directly impacts process monitoring and control. Future research will focus on developing algorithms with reduced computational complexity to enable real-time ECT system monitoring. Additionally, the potential benefits of other diffusion-regularizer functionals will be explored. The promising results of this study underscore the potential of the PMECT method to advance the applicability of ECT systems across various industrial processes and potentially improve the processes outcomes.

REFERENCES

Almutairi, Z., Al-Alweet, F. M., Alghamdi, Y. A., Almisned, O. A., & Alothman, O. Y. (2020). Investigating the Characteristics of Two-Phase Flow Using Electrical Capacitance Tomography (ECT) for Three Pipe Orientations. *Processes 2020*, **8**(1): 51. 10.3390/PR8010051

Bua, A., Kapyela, G., Massawe, L., & Maiseli, B. (2024). Edge-aware nonlinear diffusion-driven regularization model for despeckling synthetic aperture radar images. *Eurasip Journal on Image and Video Processing*, **2024**(1): 1–15. 10.1186/S13640-023-00617-/TABLES/1

Charbonnier, P., Blanc-Féraud, L., Aubert, G., & Barlaud, M. (1994). Two deterministic half-quadratic regularization algorithms for computed imaging. *Proceedings - International Conference on Image Processing, ICIP*, **2**: 168–172. 10.1109/ICIP.1994.413553

Deabes, W., & Amin, H. H. (2020). Image reconstruction algorithm based on PSO-tuned fuzzy inference system for electrical capacitance tomography. *IEEE Access*, **8**: 191875–191887. 10.1109/ACCESS.2020.3033185

Dimas, C., Alimisis, V., Uzunoglu, N., & Sotiriadis, P. (2024). Advances in Electrical Impedance Tomography Inverse Problem Solution Methods: From Traditional Regularization to Deep Learning. *IEEE Access*. 10.1109/ACCESS.2024.3382939

Egwuche, O. S., Singh, A., Ezugwu, A. E., Greeff, J., Olusanya, M. O., & Abualigah, L. (2023). Machine learning for coverage optimization in wireless sensor networks: a comprehensive review. *Annals of Operations Research 2023*, 1–67. 10.1007/S10479-023-05657-Z

Ghaly, S. M. A., Khan, M. O., Shalaby, M., Al-Snaie, K. A., & Oraiqat, M. (2023). Real Time Measurement of Multiphase Flow Velocity using Electrical Capacitance Tomography. *Engineering, Technology & Applied Science Research*, **13**(5): 11685–11690. 10.48084/ETASR.6130

Ghaly, S. M. A., Shalaby, M. Y., Al-Snaie, K., Oraiqat, M., & Khan, M. O. (2023). Image and Velocity Profile Reconstruction Using a Customized 8–16 Electrode Electrical Capacitance Tomography Sensor Based on LabVIEW Simulation. *Journal of Nanoelectronics and Optoelectronics*, **18**(6): 663–672. 10.1166/JNO.2023.3423

Gobbino, M., & Picenni, N. (2024). Monotonicity Properties of Limits of Solutions to the Semidiscrete Scheme for a Class of Perona–Malik Type Equations, **56**(2), 2034–2062. 10.1137/23M1569873

Huang, G., Sun, J., Lu, W., Peng, H., & Wang, J. (2022). ECT Image Reconstruction Method Based on Multi-Exponential Feature Extraction. *IEEE Transactions on Instrumentation and Measurement*, **71**. 10.1109/TIM.2021.3132829

Hussain, A., Faye, I., Muthuvalu, M. S., Tang, T. B., & Zafar, M. (2023). Advancements in Numerical Methods for Forward and Inverse Problems in Functional near Infra-Red Spectroscopy: A Review. *Axioms*, **12**(4): 326. 10.3390/AXIOMS12040326

Li, J., Tang, Z., Zhang, B., & Xu, C. (2023). Deep learning-based tomographic imaging of ECT for characterizing particle distribution in circulating fluidized bed. *AIChE Journal*, **69**(5): e18055. 10.1002/AIC.18055

Maiseli, B., & Abdalla, A. T. (2024). Seven decades of image super-resolution: achievements, challenges, and opportunities. *EURASIP Journal on Advances in Signal Processing 2024 2024:1*, **2024**(1): 1–21. 10.1186/S13634-024-01170-Y

Maiseli, B. J. (2020). On the convexification of the Perona–Malik diffusion model. *Signal, Image and Video Processing*, **14**(6): 1283–1291. 10.1007/S11760-020-01663-X/FIGURES/8

Mousazadeh, H., Tarabi, N., & Taghizadeh-Tameh, J. (2024). A fusion algorithm for mass flow rate measurement based on neural network and electrical capacitance tomography. *Measurement*, **231**: 114573. 10.1016/J.MEASUREMENT.2024.114573

Nombo, J., Mwambela, A., & Kisngiri, M. (2021). Analysis and Performance Evaluation of Entropic Thresholding Image Processing Techniques for Electrical Capacitance Tomography Measurement System. *Tanzania Journal of Science*, **47**(3): 928–942. 10.4314/TJS.V47I3.5

Perona, P., & Malik, J. (1990). Scale-space and edge detection using anisotropic diffusion. *IEEE Transactions on Pattern Analysis and Machine Intelligence*, **12**(7): 629–639. 10.1109/34.56205

Rafsanjani, H. K., Sedaaghi, M. H., & Saryazdi, S. (2016). Efficient diffusion coefficient for image denoising. *Computers & Mathematics with Applications*, **72**(4): 893–903. 10.1016/J.CAMWA.2016.06.005

Rajan, M. P., & Jose, J. (2022). An Efficient Discrete Landweber Iteration for Nonlinear Problems. *International Journal of Applied and Computational Mathematics*, **8**(4): 1–19. 10.1007/S40819-022-01390-6/METRICS

Rudin, L. I., Osher, S., & Fatemi, E. (1992). Nonlinear total variation-based noise removal algorithms. *Physica D: Nonlinear Phenomena*, **60**(1–4): 259–268. 10.1016/0167-2789(92)90242-F

Sharifi, M., Fourie, J., Heffernan, B., & Young, B. (2024). Developments and Applications of Electromagnetic Tomography in Process Engineering. *Chemical Engineering Research and Design*. 10.1016/J.CHERD.2024.06.018

Sun, J., Bai, X., Liu, K., Wei, J., Suo, P., & Xu, L. (2023). Bladder Volume Estimation Using 3-D Electrical Impedance Tomography Based on Fringe Field Sensing. *IEEE Transactions on Instrumentation and*

Measurement, **72**. 10.1109/TIM.2023.3277963

Suo, P., Sun, J., Li, X., Sun, S., & Xu, L. (2023). Image Reconstruction in Electrical Capacitance Tomography Using ROI-Shrinkage Adaptive Block Sparse Bayesian Learning. *IEEE Transactions on Instrumentation and Measurement*, **72**. 10.1109/TIM.2023.3314831

Tiwari, V. K., Meribout, M., Khezzar, L., Alhammadi, K., & Tarek, M. (2022). Electrical Tomography Hardware Systems for Real-time Applications: A Review. *IEEE Access*. 10.1109/ACCESS.2022.3203584

Wang, S., Sun, X., Xu, C., Bao, J., Peng, C., & Tang, Z. (2020). Investigation of a circulating turbulent fluidized bed with a fractal gas distributor by electrostatic-immune electrical capacitance tomography. *Powder Technology*, **361**, 562–570. 10.1016/J.POWTEC.2019.11.077.